

# Fe and N self-diffusion in non-magnetic Fe:N

M. Gupta,<sup>1, a)</sup> A. Gupta,<sup>1</sup> R. Gupta,<sup>2</sup> J. Stahn,<sup>3</sup> M. Horisberger,<sup>3</sup> and A. Wildes<sup>4</sup>

<sup>1)</sup> UGC-DAE Consortium for Scientific Research, University Campus, Khandwa Road, Indore-452 001, India

<sup>2)</sup> Acropolis Institute of Technology and Research, Manglia Square, Indore-453 771, India

<sup>3)</sup> Laboratory for Neutron Scattering, ETH Zurich and Paul Scherrer Institut, CH-5232 Villigen PSI, Switzerland

<sup>4)</sup> Institut Laue-Langevin, rue des Martyrs, 38042 Grenoble Cedex, France

(Dated: 2 April 2024)

Fe and N self-diffusion in non-magnetic Fe:N has been studied using neutron reflectivity. The isotope labelled multilayers,  $[\text{Fe:N}/^{57}\text{Fe:N}]_{10}$  and  $[\text{Fe:N}/\text{Fe}^{15}\text{N}]_{10}$  were prepared using magnetron sputtering. It was remarkable to observe that N diffusion was slower compared to Fe while the atomic size of Fe is larger compared to N. An attempt has been made to understand the diffusion of Fe and N in non-magnetic Fe:N.

Iron nitrides (Fe:N) show a variety of structures and magnetic properties with a variation in the nitrogen content. With an increasing atomic percentage (*at.*% N), their major phases are:  $\text{Fe}_{16}\text{N}_2$ ,  $\text{Fe}_4\text{N}$ ,  $\text{Fe}_3\text{N}$ ,  $\text{Fe}_2\text{N}$ , FeN and  $\text{Fe}_3\text{N}_4$ . For  $\leq 25$  *at.*% N, the Fe:N phases are magnetic.<sup>1</sup> A lot of attention has been driven to  $\alpha'' - \text{Fe}_{16}\text{N}_2$  ( $\sim 11$  *at.*% N) due to the presence of the so-called giant magnetic moment in this compound.<sup>2,3</sup> Around 20 *at.*% N,  $\gamma' - \text{Fe}_4\text{N}$  phase is formed which has a well-defined magnetic properties and crystal structure.<sup>4</sup> Very recently the  $\gamma'$  phase has received a lot of interest due to its chemical inertness and mechanically hard surfaces making it a suitable alternative to pure Fe in magnetic devices.<sup>4-8</sup> Between 25-33 *at.*% N the Fe:N are known as  $\epsilon - \text{Fe}_x\text{N}$  ( $2 \leq x \leq 3$ ), and as N *at.*% increases from 25% to 33%, the phase changes from ferromagnetic  $\text{Fe}_3\text{N}$  to paramagnetic  $\text{Fe}_2\text{N}$  at room temperature. Earlier it was not possible to produce the Fe:N phases containing more than 33 *at.*% N but by using reactive sputtering<sup>9-11</sup> and pulsed laser deposition techniques,<sup>12</sup> the Fe:N phases with  $>33$  *at.*% N were produced. Around 50 *at.*% N, the FeN phases have cubic ZnS and/or NaCl-type structures which are known as  $\gamma''$  and/or  $\gamma'''$ . The  $\text{Fe}_3\text{N}_4$  phase with even more than 50 *at.*% N was predicted by Ching *et al.*<sup>13</sup>, but has not been evidenced experimentally.

Recently, the  $\epsilon - \text{Fe}_2\text{N}$  and  $\gamma''/\gamma'''$  phases have been used as a precursor to prepare  $\gamma' - \text{Fe}_4\text{N}$  phase for its use in the spintronic devices.<sup>5-7</sup> In the present work, we have prepared single phase  $\epsilon - \text{Fe}_2\text{N}$  and  $\gamma''' - \text{FeN}$  compounds and studied the self-diffusion of Fe and N. A proper understanding of the stability and nitride formation requires the knowledge of both Fe and N self-diffusion at atomic length scales. However, there are no studies on measurements of both Fe and N self-diffusion in non-magnetic Fe:N. Conventional techniques to measure self-diffusion (e.g. secondary ion mass spectroscopy, radioactive tracer etc.) have depth resolutions of several

nm. Therefore, to measure diffusion at nanometer length scale, a technique with depth resolution in the sub-nm regime is necessary.<sup>14</sup> Here, the method of choice is neutron reflectometry (NR), which in addition is sensitive to isotopic contrast: neutron scattering length for natural Fe and  $^{57}\text{Fe}$  are 9.45 and 2.3 fm, and for natural N and  $^{15}\text{N}$  9.36 and 6.6 fm, respectively.

The samples were prepared at room temperature by DC magnetron sputtering using either a mixture of Ar and  $\text{N}_2$  (samples A), or with pure  $\text{N}_2$  (samples B) as sputtering gas. During the deposition the total gas flow was kept constant at 10 standard  $\text{cm}^3/\text{min}$  (sccm) and the sputtering power at 50 W. The actual thicknesses (obtained using NR) and gas flow parameters are; Samples (A):  $[\text{Fe:N}(7.5 \text{ nm})/^{57}\text{Fe:N}(4.5 \text{ nm})]_{10}$ ,  $[\text{Fe:N}(6.4 \text{ nm})/\text{Fe}^{15}\text{N}(3.2 \text{ nm})]_{10}$  multilayers deposited using sputter gas ( $\text{N}_2 + \text{Ar}$ ) each at 5 sccm. And samples (B):  $[\text{Fe:N}(10.2 \text{ nm})/^{57}\text{Fe:N}(5.2 \text{ nm})]_{10}$ ,  $[\text{Fe:N}(10.6 \text{ nm})/\text{Fe}^{15}\text{N}(5.2 \text{ nm})]_{10}$  multilayers using 10 sccm  $\text{N}_2$  as sputter gas. The multilayer with  $^{57}\text{Fe}$  was deposited by alternatively sputtering Fe/ $^{57}\text{Fe}$  enriched targets and the  $^{15}\text{N}$  multilayer was prepared using the same Fe target but switching between N/ $^{15}\text{N}$  gases. A residual gas analyzer was installed in the sputtering chamber to monitor the isotope abundance of nitrogen. The samples were characterized using x-ray diffraction (XRD) using Cu-K $\alpha$  x-rays while thermal stability was examined using differential scanning calorimetry (DSC). The local environment of  $^{57}\text{Fe}$  atoms was probed using conversion electron Mössbauer spectroscopy (CEMS). The NR measurements were performed at the reflectometers AMOR at SINQ/PSI<sup>15</sup>, and D17 at ILL<sup>16</sup>, both in the time-of-flight mode.

The CEMS and XRD patterns of samples A and B are shown in fig. 1 (a)-(d). The XRD pattern of sample A (fig. 1b), shows peaks corresponding to  $\epsilon - \text{Fe}_x\text{N}$  with hexagonal closed pack structure. The CEMS spectrum of this sample (fig. 1a) shows an asymmetric doublet which was fitted using two doublets corresponding to Fe-III and Fe-II sites with isomer shifts of  $0.43 \pm 0.002$  and  $0.37 \pm 0.002 \text{ mm/s}$ ; quadrupole splitting of  $0.24 (\pm 0.002)$  and  $0.50 \pm 0.004 \text{ mm/s}$  and the relative area ratio of 69:31,

<sup>a)</sup> Electronic mail: mgupta@csr.ernet.in

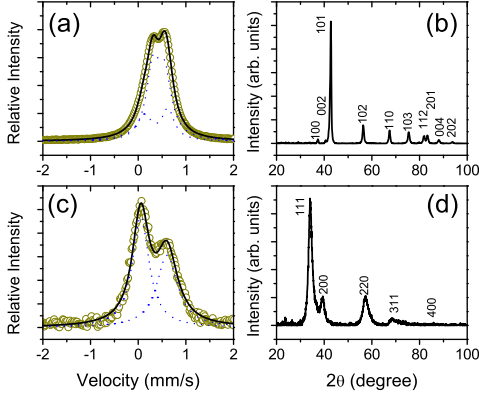


FIG. 1. (Color online) CEMS pattern of sample A (a) and sample B (c). XRD pattern of sample A (b) and sample B (d).

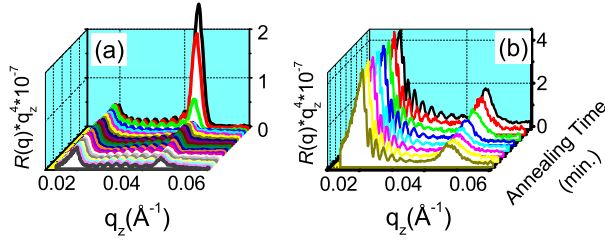


FIG. 2. (Color online) Neutron reflectivity pattern (reflectivity  $R$ , multiplied by  $q_z^4$  for better visibility of Bragg peak) of sample B measured at 463 K for different annealing time taken with an interval of 30 min. The time dependence of Fe (a) and N diffusivity (b) can be seen.

respectively. The fitted parameters matches well with the reported values and using the relative area ratio, we obtain the value of  $x = 2.23$  following the procedure given in ref.<sup>9</sup>

The XRD pattern of the sample B (fig. 1d) shows all the peaks corresponding to  $\gamma'''$ -FeN phase with lattice parameter  $a = 0.454 \pm 0.001$  nm. The CEMS pattern of this sample (fig. 1c) shows an asymmetric doublet and was fitted using two singlets with isomer shifts of  $0.05 \pm 0.002$  and  $0.6 \pm 0.003$  mm/s. The XRD and CEMS parameters match well with the values obtained by Jouanny *et al.*<sup>17</sup> for  $\gamma'''$ -FeN having ZnS-type structure with  $\approx 50_{at.}\%$  N. The average grain size calculated using the Scherrer formula for the most intense peak in sample A and B are 16 nm and 5 nm, respectively.

The thermal stability of the samples was studied using XRD and DSC. In the temperature range of 373-573 K there was no appreciable change in the XRD patterns and DSC measurements showed a strong exothermic peak at 650 K, indicating out-diffusion of nitrogen as observed in an earlier study.<sup>18</sup> Therefore 523 K was chosen as the maximum annealing temperature for the diffusion measurements. The  $^{57}\text{Fe}$  and  $^{15}\text{N}$  periodicity gives rise to Bragg peaks in the NR pattern, which become less sharp as the multilayers are annealed. Some representative NR patterns for sample B at 463 K at different annealing time

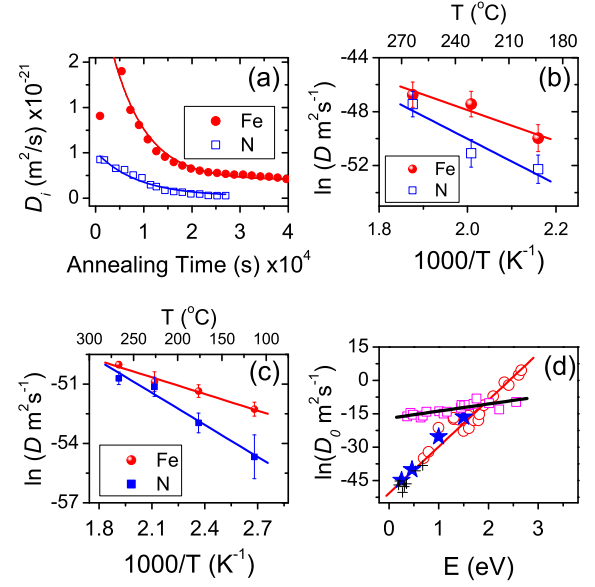


FIG. 3. (Color online) Time dependence of Fe and N instantaneous diffusivity for sample B at 463 K (a). Arrhenius behavior of Fe and N diffusivity for sample B (b) and for sample A (c). The correlation between  $\ln D_0$  and  $E$  (d) for crystalline (□) and amorphous (○) alloys<sup>20</sup>. The star (★) represents data obtained in the present work and (+) corresponds to the values obtain in crystalline thin film multilayers.<sup>21</sup>

TABLE I. Parameters for Fe:N samples.

Sample	A	B
Composition	$\epsilon - \text{Fe}_{2.23}\text{N}$	$\gamma''' - \text{FeN}$
$E_{\text{Fe}}$ (eV)	$0.25 \pm 0.03$	$1.0 \pm 0.2$
$E_{\text{N}}$ (eV)	$0.46 \pm 0.08$	$1.5 \pm 0.3$
$\ln D_{0_{\text{Fe}}} (\text{m}^2/\text{s})$	$-44 \pm 1$	$-25 \pm 10$
$\ln D_{0_{\text{N}}} (\text{m}^2/\text{s})$	$-41 \pm 2$	$-16 \pm 10$

(with a step of 30 min) are shown in fig. 2 (a) and (b) for Fe and N contrast. The pattern was multiplied with  $q_z^4$  to remove the decay due to Fresnel's reflectivity. The decay of the Bragg peak intensity can be used to calculate instantaneous diffusivity ( $D_i$ ) using the expression:<sup>19</sup>  $\ln[I(t)/I(0)] = -8\pi^2 n^2 D_i t / d^2$  where  $I(0)$  is the intensity of the  $n^{\text{th}}$  order Bragg peak at time  $t = 0$  (before annealing) and  $d$  is the bilayer thickness. As the structure tends to relax, the time averaged diffusivity is defined by:<sup>20</sup>  $\bar{D} = \frac{1}{t} \int_0^t D_i(t') dt'$ . Assuming an exponential law for relaxation,  $D_i(t) = \text{Const.} \exp(-t/\tau) + D$ , where  $D$  is diffusivity in the relaxed state and  $\tau$  is the relaxation time. Using this relation the diffusivities in the structurally relaxed state were obtained and are shown in fig. 3 (a). The temperature dependence of diffusivity obtained in the structurally relaxed state follows an Arrhenius-type behavior as shown in fig. 3 (b) for sample B. Similarly, for sample A, the Arrhenius behavior for Fe and N diffusivity is shown in fig. 3 (c). The straight line fit to the data obtained using:  $D = D_0 \exp(-E/k_B T)$ , yields the pre-exponential factor ( $D_0$ ) and activation energy ( $E$ ) which are given in table I with  $k_B$  being Boltzman's constant.

It is known that a correlation exists between  $\ln D_0$  and

$E$ , which is followed in all class of materials and indicates the involved diffusion mechanism.<sup>20</sup> While including our values of  $E$  and  $\ln D_0$  in this correlation (fig. 3d), we find that our values follow this correlation well for diffusion in amorphous alloys. With a straight line fit of the values obtained for amorphous alloys with our data, we can calculate the entropy ( $\Delta S$ ) for diffusion following the procedure given in ref.<sup>14</sup> The calculated values of  $\Delta S$  for Fe and N diffusion are  $5 k_B$  and  $19 k_B$  for sample *A* and  $9 k_B$  and  $28 k_B$  for sample *B*, respectively. In crystalline systems the value of  $\Delta S$  is typically  $(3-5) k_B$  corresponding to interstitialcy or monovacancy mechanism.<sup>21</sup> The relatively large values of  $\Delta S$  indicate that the diffusion mechanism in the present case is more similar to amorphous alloys where collective type diffusion occurs involving a group of atoms. As we see from the XRD measurements, the grain sizes are rather small (16 nm and 5 nm in sample *A* and *B*). If the diffusion takes place from the grain boundaries which are not so well-ordered, the diffusion mechanism will lead to a situation similar to amorphous alloys.<sup>22</sup> In an earlier study, we measured the Fe self-diffusion in a nearly equiatomic amorphous and nonmagnetic FeN alloy<sup>18</sup> and found  $E_{Fe}=1.3\pm 0.2$  eV which is close to  $E_{Fe}=1\pm 0.2$  eV for sample *B*. Therefore nearly similar values of  $E$  in amorphous and crystalline FeN thin films indicate a similar type of diffusion mechanism which is independent of the structure.

The comparison of diffusivity in samples *A* and *B* reveals that the values of  $E$  are greater in sample *B*. This indicates a slower diffusion of Fe or N in sample *B* as compared to sample *A*. Looking at the enthalpies of formation ( $\Delta H^\circ$ ), the values for FeN are the lower as compared to  $Fe_2N$  or other Fe:N phases.<sup>23</sup> This means that FeN is expected to be more stable as compared to  $Fe_2N$  and therefore  $E$  for Fe and N self-diffusion should be high in FeN as compared to  $Fe_2N$ . Though the differences in the obtained values of diffusivity in both samples can be understood in terms of energetics of iron nitrides, it is the difference between the Fe and N self-diffusion which is counter intuitive as the atomic size of Fe ( $r_{Fe} = 0.1274$  nm) is larger than N ( $r_{Fe}/r_N \approx 1.6$ ). Therefore, it is expected that N should be diffusing faster than Fe as was observed in a N-poor magnetic Fe:N.<sup>24</sup> In the literature we see that atomic size dependency (i.e. smaller atoms diffuses faster) is observed metal-metal and metal-metalloid amorphous alloys<sup>20,25</sup>. However, in case of phosphorus self-diffusion in  $Fe_{40}Ni_{40}P_{14}B_6$  and in  $Pd_{43}Cu_{27}Ni_{10}P_{20}$  metallic glass the diffusion coefficient of P was found to be smaller compared to Fe and Cu.<sup>26,27</sup> It was suggested that the local chemical interactions around P (strong covalent bonds) are more important for the diffusion than the atomic size dependence of constituent elements in the alloy. In the periodic table N and P are in the same group (VB) and the anomaly observed for P self-diffusion can be extended to N self-diffusion in nonmagnetic Fe:N phases. However, as the temperature increases we observed that the difference between Fe and N diffusivity becomes smaller.

In conclusion, we measured Fe and N self-diffusion in non-magnetic  $\epsilon - Fe_{2.23}N$  and  $\gamma''' - FeN$  compounds. The activation energy of Fe and N is higher in  $\gamma''' - FeN$  than in  $\epsilon - Fe_{2.23}N$ . However, the diffusivity of N is smaller compared to Fe in both samples. The differences in Fe and N diffusivity can not be understood in terms of atomic size of Fe and N.

We acknowledge DST for providing financial support to carry out NR experiments under its scheme ‘Utilization of International Synchrotron Radiation and Neutron Scattering facilities’. A part of this work was performed under the Indo Swiss Joint Research Programme with grant no. INT/SWISS/JUAF(9)/2009.

- <sup>1</sup>X. Wang, W. T. Zheng, H. Tian, S. S. Yu, and L. L. Wang, J. Magn. Magn. Mat. **283**, 282 (2004).
- <sup>2</sup>T. K. Kim and M. Takahashi, Appl. Phys. Lett. **20**, 492 (1972).
- <sup>3</sup>M. Komuro, Y. Kozono, M. Hanazono, and Y. Sugita, J. Appl. Phys. **67**, 5126 (1990).
- <sup>4</sup>C. Navío, J. Alvarez, M. J. Capitan, D. Eciija, J. M. Gallego, F. Yndurain, and R. Miranda, Phys. Rev. B **75**, 125422 (Mar 2007).
- <sup>5</sup>C. Navío, J. Alvarez, M. J. Capitan, J. Camarero, and R. Miranda, Appl. Phys. Lett. **94**, 263112 (2009).
- <sup>6</sup>C. Navío, J. Alvarez, M. J. Capitan, F. Yndurain, and R. Miranda, Phys. Rev. B **78**, 155417 (Oct 2008).
- <sup>7</sup>L. de Wit, T. Weber, J. S. Custer, and F. W. Saris, Phys. Rev. Lett. **72**, 3835 (1994).
- <sup>8</sup>J. M. Gallego, D. O. Boerma, R. Miranda, and F. Yndurain, Phys. Rev. Lett. **95**, 136102 (Sep 2005).
- <sup>9</sup>P. Schaaf, C. Illgner, M. Niederrenk, and K. P. Lieb, Hyp. Int. **95**, 199 (1995).
- <sup>10</sup>R. Gupta and M. Gupta, Phys. Rev. B **72**, 024202 (2005).
- <sup>11</sup>A. Filippetti and W. E. Pickett, Phys. Rev. B **59**, 8397 (Apr 1999).
- <sup>12</sup>M. Gupta, A. Gupta, P. Bhattacharya, P. Misra, and L. M. Kukreja, J. Alloys and Compds. **326**, 265 (2001).
- <sup>13</sup>W. Y. Ching, Y. N. Xu, and P. Rulis, Appl. Phys. Lett. **80**, 2904 (2002).
- <sup>14</sup>M. Gupta, A. Gupta, J. Stahn, M. Horisberger, T. Gutberlet, and P. Allenspach, Phys. Rev. B **70**, 184206 (2004).
- <sup>15</sup>M. Gupta, T. Gutberlet, J. Stahn, P. Keller, and D. Clemens, Pramana J. Phys **63**, 57 (2004).
- <sup>16</sup>R. Cubitt and G. Fragneto, Appl. Phys. A **74**, 329 (2002).
- <sup>17</sup>I. Jouanny, P. Weisbecker, V. Demange, M. Grafouté, O. P. na, and E. Bauer-Grosse, Thin Solid Films **518**, 1883 (2010).
- <sup>18</sup>M. Gupta, A. Gupta, S. Rajagopalan, and A. K. Tyagi, Phys. Rev. B **65**, 214204 (2002).
- <sup>19</sup>M. P. Rosenblum, F. Spaepen, and D. Turnbull, Appl. Phys. Lett. **37**, 184 (1980).
- <sup>20</sup>F. Faupel, W. Frank, M. P. Macht, H. Mehrer, K. Rätzke, H. Schober, S. K. Sharma, and H. Teichler, Rev. Mod. Phys. **75**, 237 (2003).
- <sup>21</sup>W.-H. Wang, H. Y. Bai, M. Zhang, J. H. Zhao, X. Y. Zhang, and W. K. Wang, Phys. Rev. B **59**, 10811 (Apr 1999).
- <sup>22</sup>A. Gupta, M. Gupta, U. Pietsch, S. Ayachit, S. Rajagopalan, A. Balamurgan, and A. Tyagi, J. Non. Cryst. Solids **343**, 39 (2004).
- <sup>23</sup>F. Tessier, A. Navrotsky, R. Niewa, A. Leineweber, H. Jacobs, S. Kikkawa, M. Takahashi, F. Kanamaru, and F. J. DiSalvo, Solid State Sciences **2**, 457 (2000).
- <sup>24</sup>S. Chakravarty, M. Gupta, A. Gupta, S. Rajagopalan, A. Balamurgan, A. Tyagi, U. Deshpande, M. Horisberger, and T. Gutberlet, Acta Materialia **57**, 1263 (2009).
- <sup>25</sup>R. W. Cahn, J. E. Evetts, J. Patterson, R. E. Somekh, and C. K. Jackson, J. Mater. Sci. **15**, 702 (1980).
- <sup>26</sup>Y. Yamazaki, T. Nihei, J. Koike, and T. Ohtsuki, Proc. 1<sup>st</sup> Int. Conf. Diff. Sol. Liq. vol. **II**, 831 (2005).

<sup>27</sup>P. Valenta, K. Maier, and H. K. K. Freitag, Phys. Stat. Sol. B **106**, 129 (1981).